THE JOURNAL OF PHYSICAL CHEMISTRY C

ARTICLE

pubs.acs.org/JPCC

Coupled Optical and Electronic Modeling of Dye-Sensitized Solar Cells for Steady-State Parameter Extraction

Sophie Wenger,[¶,†] Matthias Schmid,[‡] Guido Rothenberger,[†] Adrian Gentsch,[‡] Michael Grätzel,[†] and Jürgen O. Schumacher*[,‡]

[†]Laboratory of Photonics and Interfaces, Ecole Polytechnique Fédérale de Lausanne, EPFL-SB-ISIC-LPI, Station 6, 1015 Lausanne, Switzerland

[‡]Institute of Computational Physics, Zurich University of Applied Sciences (ZHAW), Wildbachstrasse 21, 8401 Winterthur, Switzerland

Supporting Information

ABSTRACT: The design and development of dye-sensitized solar cells (DSCs) is currently often realized on an empirical basis. In view of assisting in this optimization process, we present the framework of a model which consists in a coupled optical and electrical model of the DSC. The experimentally validated optical model, based on a ray-tracing algorithm, allows accurate determination of the *internal quantum efficiency* of devices, an important parameter that is not easily estimated. Coupling the output of the optical model—the dye absorption rate—to an electrical model for charge generation, transport, and first-order (linear) recombination allows extraction of a set of intrinsic parameters from steady-state photocurrent measurements, such as the diffusion length or the dye electron injection efficiency. Importantly, the sources of optical and electric losses in the device can be separated and quantified (i.e., transmittance, reflectance, absorptance, charge injection, recombination, and potential losses). The model has been validated for two dye systems (Z907 and C101) and the strong effect of the presence of Li^+ ions in the electrolyte on intrinsic parameters is confirmed. This optoelectronic model of the DSC is a significant step toward a future systematic model-assisted optimization of DSC devices.

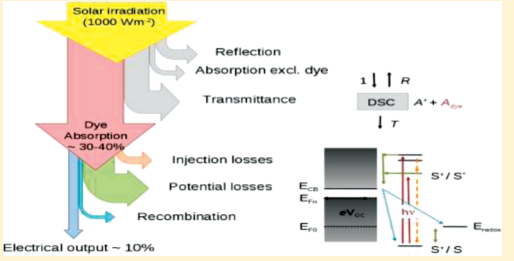

INTRODUCTION

Dye-sensitized solar cells (DSCs) can convert solar radiation into electricity efficiently and cost-effectively by means of a light-harvesting sensitizer anchored to a high surface area mesoporous semiconductor film.[1] Record efficiencies of over 11% have been achieved with ruthenium-complex sensitizers on laboratory-scale devices,[2−4] but progress in efficiency enhancement has been slow in the past years. The optimization of crystalline silicon solar cells is routinely assisted by numerical simulations (e.g., with the program PC1D[5]). Various simulators also exist for thin-film solar cells[6] and organic solar cells.[7] The materials and device optimization of the DSC, however, are often addressed with an empirical approach. Clearly, a comprehensive optoelectronic DSC simulator would accelerate device development. With this work, we attempt to lay the foundations for a coupled optical and electrical DSC simulator, putting a focus on the accurate description of the optics in the device.[8]

The DSC is a nanostructured electrochemical device (Figure 1). Sunlight is absorbed by a photoactive sensitizer ("dye") attached to a thin mesoporous TiO_2 film ($x < 12\ \mu m$). The photoexcited dye injects an electron into the TiO_2 conduction band and is rapidly regenerated by a mediator redox couple in the electrolyte, which permeates the pores. The injected electron diffuses through the TiO_2 network to a transparent conducting electrode (fluorine-doped tin oxide, FTO) and migrates through an external electric circuit to the counter electrode, where it regenerates the oxidized mediator.

The optical modeling of the device is complicated by the presence of the mixed mesoporous medium comprising three absorbers (TiO_2, dye, and electrolyte). Often, the optics in the device and the charge generation function in the photoactive layer are calculated using a simplified, Lambert−Beer-type, exponential absorption.[9−11] This approach, however, does not account for multiple reflections occurring at interfaces in the device and neglects coherence effects in thin films (e.g., FTO layers). We use a ray-tracing algorithm to accurately calculate the absorption of light in a complete device. Coherence effects in the FTO layer are treated with the transfer matrix method. The light intensity perpendicular to a six-layer stack (along the x axis in Figure 1) is calculated using coherent and incoherent optics. The fraction of the incident light absorbed by the stained TiO_2 layer gives the spatially resolved charge generation function.

Standard materials, which have been used in our laboratory and other research groups for several years, were selected for the optical analysis. We have characterized the layers, in particular the FTO electrodes and the absorption coefficient of the dye under operating conditions (i.e., adsorbed to the TiO_2 surface and in an electrolyte solvent environment), as thoroughly as

Received: December 5, 2010
Revised: February 20, 2011
Published: May 03, 2011

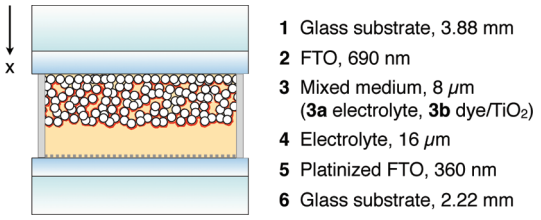

Figure 1. Device structure of the dye-sensitized solar cell depicting the six layers used to model the optics in the device.

possible. The validity and utility of the model are demonstrated with test devices using standard or benchmark ruthenium-based dyes: the well-known Z907 dye[12] and the high absorptivity C101 dye.[4]

The accurately calculated charge generation function is coupled to a linear continuity equation for free electrons in the TiO_2 film. Using the analytical solution, we calculate steady-state properties of the device under constant illumination at short-circuit conditions, i.e., photocurrent and external quantum efficiency, and compare them to measured values. In particular, we can extract values for electron diffusion length and charge injection efficiency from excited dye states into the TiO_2 conduction band.[10,11]

Under the chosen experimental conditions, nearly all electrons are collected at short circuit. In this case the nonlinear recombination of electrons can be well approximated using the first order rate equation.[13] An analytical expression for the conduction band electron concentration can thus be calculated solving this linear differential equation. Nonlinear models have been proposed in the literature to account for the light intensity dependence of the external quantum efficiency at very low intensity or the observed deviation from an "ideal" slope of k_BT/e when the open circuit potential is graphed as a function of the natural logarithm of the incident light flux. These models lead to differential equations that must be solved numerically. For instance, a power law recombination rate with an exponent of the concentration smaller than 1 describes well some the experimental findings but raises the question of the physical interpretation of the rate equation.[14,15] Alternatively, an additional recombination route via intraband surface states[16] may exist. A model which, in addition to conduction band electrons, considers also localized bulk and surface states, with a back reaction from the latter, may lead to a nonlinear behavior.

The paper is organized as follows. In the next section we introduce the coupled optical and electrical model. The device preparation and the optical and photovoltaic characterizations are described in the Experimental Section. The comparison of the experimental data with the simulations and the loss analysis are reported in the Results and Discussion section, which is followed by a Conclusions section.

THEORY

Optical Model. The optical model calculates the light intensity along the x axis of a six-layer stack shown in Figure 1. A distinction is made between thick layers whose optics is treated incoherently and thin layers where coherent optics applies. The x axis is perpendicular to the interfaces. The model is based on a ray-tracing algorithm using geometrical, i.e. incoherent, optics.[17] The ray-tracer randomly generates light rays, which are geometrically traced through the stack, until the intensity of a ray is

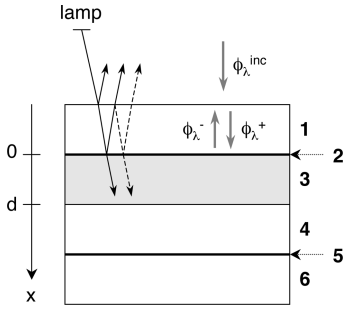

Figure 2. Schematic of the six layer stack used for the optical model. Bold numbers refer to the layers described in Figure 1. Incident rays are reflected and transmitted at interfaces and traced throughout the stack (thin dark arrows). Rays are perpendicular to the interfaces in the model and drawn at an angle for visualization only. For a given wavelength λ, ϕ_λ^{inc} is the spectral photon flux density incident on the stack, $\phi_\lambda^+(x)$ is the forward flux (the sum of all forward propagating rays), and $\phi_\lambda^-(x)$ is the backward flux (the sum of all backward propagating rays) at position x. The two thin FTO films **2** and **5** are represented by optically thin interfaces. Coherent optics is used to calculate the reflectance and transmittance coefficients of the FTO films. Layer **3** constitutes the mixed medium (mesoporous TiO_2, dye, electrolyte) with thickness d.

below a preset threshold value. In this work, the rays are always perpendicular to the interfaces. The tracing procedure is repeated for different discrete wavelength values. At each interface between thick layers, the ray is split into a transmitted and a reflected beam. The reflectance and transmittance coefficients at the interfaces are calculated from the experimentally determined complex refractive indices of the layers ($\tilde{n}_i(\lambda) = n_i(\lambda) + ik_i(\lambda)$, $1 \le i \le 6$). In an absorbing medium of thickness d_i, the ray intensity is attenuated by the factor $\exp(-\alpha_i(\lambda)\, d_i)$, where $\alpha_i(\lambda) = 4\pi k_i/\lambda$ is the absorption coefficient. Thus, the incident ray is split into a "tree" of rays, which are all traced individually.

The two thin FTO films (layers **2** and **5**) must be treated using coherent optics, since their thickness is in the order of the sunlight coherence length (~600 nm).[18] The transmittance and reflectance coefficients of the two thin FTO films are calculated with a transfer matrix approach.[19,20] The mixed incoherent−coherent stack is then modeled as shown in Figure 2.

The spectral absorption rate of photons per unit volume, $G_\lambda(x)$, for a given wavelength λ at position x is given by the derivative of the net spectral photon flux density $\phi_\lambda(x)$. By use of the superposition principle, $\phi_\lambda(x)$ is calculated from the sum of the forward flux $\phi_\lambda^+(x)$, which includes all rays propagating in the forward direction, and the backward flux $\phi_\lambda^-(x)$, which includes all rays propagating in the backward direction. The spectral photon absorption rate then is

$$G_\lambda(x) = -\frac{d\phi_\lambda^+(x)}{dx} + \frac{d\phi_\lambda^-(x)}{dx} \quad (1)$$

It is convenient to normalize $G_\lambda(x)$ with respect to an arbitrary incident spectral photon flux density ϕ_λ^{inc}

$$g(\lambda, x) = \frac{G_\lambda(x)}{\phi_\lambda^{inc}} \quad (2)$$

Light propagation and absorption in the mesoporous medium of layer **3** constitute a special case. For this layer, the real part n_3 of the complex index of refraction ($\tilde{n}_3 = n_3 + ik_3$) is estimated from the Bruggeman effective medium approximation.[21] The porous medium is described as a mixture of medium **3a** ($\tilde{n}_{3a}$), the

electrolyte, and medium **3b** ($\tilde{n}_{3b}$), a fictitious TiO_2/dye phase. The effective complex index of refraction, $\tilde{n}_3$, then satisfies

$$P\frac{\tilde{n}_{3a}^2-\tilde{n}_3^2}{\tilde{n}_{3a}^2+2\tilde{n}_3^2}+(1-P)\frac{\tilde{n}_{3b}^2-\tilde{n}_3^2}{\tilde{n}_{3b}^2+2\tilde{n}_3^2}=0 \quad (3)$$

where P is the porosity of the mesoporous film. The parameters P, n_{3a}, n_{3b}, k_{3a}, and k_3 are known from experiments or literature (see Experimental Section). k_3 is experimentally determined using a four-flux model analysis[22] on transmittance and reflectance spectra of a simplified stack, where the two FTO electrodes (**1**/**2** and **5**/**6**) are replaced by microscope glass slides. Details on the four-flux analysis are given in the Supporting Information. The unknown parameters n_3 and k_{3b} are back-calculated from eq 3. k_{3b}, however, is unneeded for the remaining calculations, since it represents the extinction coefficient of a bulk dye/TiO_2 medium with $P \rightarrow 0$.

Between $x = 0$ and $x = d$, $g(\lambda,x)$ includes absorption by the dye and the electrolyte. The absorption by the dye only (g^{dye}) is calculated using

$$g^{dye}(\lambda,x)=\frac{\alpha_{dye}(\lambda)}{\alpha_3(\lambda)}g(\lambda,x) \quad \text{for } 0\le x\le d \quad (4)$$

Here, $\alpha_3 = 4\pi k_3/\lambda$ is the effective absorption coefficient of all absorbers in layer **3**. α_3 and α_{dye} are determined from a four-flux model analysis (see Supporting Information).

By integrating $g^{dye}(\lambda,x)$ over the TiO_2 film thickness interval $[0, d]$, where d is the film thickness, we find the total fraction of absorbed light by the dye in the film at wavelength λ (or the maximum achievable external quantum efficiency)

$$f_{abs}(d,\lambda)=\int_0^d g^{dye}(\lambda,x)\,dx \quad (5)$$

The dye absorption rate for a given incident photon flux ϕ_λ^{inc} is

$$G_\lambda^{dye}(x)=\phi_\lambda^{inc}g^{dye}(\lambda,x) \quad (6)$$

We assume that the efficiency for electron injection from excited dye states into the TiO_2 conduction band is independent of wavelength ($\eta_{inj}(\lambda) = \eta_{inj}$). The spatially resolved electron generation rate is then

$$G_e(x)=\eta_{inj}G^{dye}(x) \quad (7)$$

where

$$G^{dye}(x)=\int_0^\infty G_\lambda^{dye}(x)\,d\lambda$$

In addition, we obtain the maximum achievable short circuit current density using

$$j_{max}=e\int_0^d G_e(x)\,dx \quad (8)$$

where e is the elementary charge.

The optical model does not account for scattering in its present form. It has been validated with TiO_2 films made from 20 nm sized particles that scatter light only weakly. An extension of the present optical model to scattering layers can be envisaged. An angular distribution of ray propagation directions must then be considered, instead of rays propagating only perpendicularly to the interfaces. Possible absorption or scattering events in a layer, and refraction, reflection, or scattering at an interface determine then the fate of a particular ray. Such an extension of the model comes, however, at the cost of a considerable increase of the complexity of the program.

Electrical Model. The output of the optical model, the charge generation function $G_e(x) = \eta_{inj}G^{dye}(x)$, is coupled to an electrical model for free charge carriers. Here, for simplicity, we do not include ionic transport in the electrolyte and the reduction of triiodide at the counter-electrode. The electrical model is based on the stationary continuity equation for the electron number density $n(x)$ in the conduction band of the TiO_2 layer and on a purely diffusive transport equation for the electrical current density j.[23] If the quasi-equilbrium approximation is used (one single quasi-Fermi level for conduction band and trapped electrons), then, under steady-state conditions, the continuity equation does not include terms due to trapping/detrapping, provided that there is no back reaction between trapped electrons and species present in the electrolyte.[24] In the simplest (ideal) model case, only electrons from the conduction band can recombine with triiodide in the electrolyte, and the recombination rate is taken to be first order in $n(x)$. This leads to an inhomogeneous linear differential equation for $n(x)$

$$L^2\frac{d^2n}{dx^2}-(n(x)-\overline{n})+\tau G_e(x)=0 \quad (9)$$

Here, $L = (D\tau)^{1/2}$ is the constant electron diffusion length, τ is the electron lifetime, and $\overline{n}$ is the electron number density at equilibrium in the dark. The electron number density in the dark is given by

$$\overline{n}=N_c\frac{2}{\sqrt{\pi}}F_{1/2}\left(\frac{E_{F0}-E_c}{kT}\right) \quad (10)$$

where N_c is the effective density of conduction band states, E_c is the conduction band energy, and E_{F0} is the Fermi level in the dark, which is equilibrated with the redox potential of the iodide/triiodide couple. $F_{1/2}$ is the Fermi−Dirac integral[25] defined as

$$F_{1/2}(\eta)=\int_0^\infty\frac{\sqrt{x}}{1+\exp(x-\eta)}\,dx \quad (11)$$

The boundary conditions to eq 9 are

$$n(0)=N_c\frac{2}{\sqrt{\pi}}F_{1/2}\left(\frac{E_{F0}+eV-E_c}{kT}\right) \quad (12)$$

and

$$\left.\frac{dn}{dx}\right|_{x=d}=0$$

where V is the photovoltage. The photovoltage corresponds to the internal cell voltage given by

$$V=\frac{1}{e}(E_{Fn}(0)-E_{F0}) \quad (13)$$

where $E_{Fn}(0)$ is the electron quasi-Fermi energy at $x = 0$. Setting $V = 0$ we obtain the short-circuit case.

The general solution of (9) is given by

$$n(x)=ae^{-x/L}+be^{x/L}+\overline{n}-\tau\int_0^d\mathcal{G}(x-y)G_e(y)\,dy \quad (14)$$

Here, a and b are constants determined by the boundary conditions. The last two terms comprise the particular solution

of the differential eq 9. Because the generation rate $G_e(x)$ is known in numerical form, the particular solution is most conveniently expressed using Green's function $\mathscr{G}(x)$ of eq 9. (The Green's function of (9) is calculated by using the Fourier transform and is given by

$$\mathscr{G}(x) = -\frac{1}{2L}[H(-x)\exp(x/L) + H(x)\exp(-x/L)]$$

where $H(x)$ is the unit step function.) From the complete solution for $V = 0$, the current density at short circuit can be calculated by

$$j_{sc} = eD\left.\frac{dn}{dx}\right|_{x=0} \quad \text{for } V = 0 \tag{15}$$

For details of these calculations we refer the reader to the Supporting Information.

The external quantum efficiency (EQE) is simulated using monochromatic light of wavelength λ_0 and incident photon flux density ϕ^{inc} to calculate the injected charge generation rate

$$G_e^{\delta}(x) = \eta_{inj} G^{dye,\delta} = \eta_{inj}\phi^{inc}\int_0^{\infty} \delta(\lambda-\lambda_0) g^{dye}(\lambda,x)\, d\lambda \tag{16}$$

$$= \eta_{inj}\phi^{inc} g^{dye}(\lambda_0,x) \tag{17}$$

The EQE at wavelength λ_0 is then derived from the calculated $j_{sc}(\lambda_0)$ by inserting $G_e^{\delta}(x)$ in eq 14

$$\mathrm{EQE}(\lambda_0) = \frac{j_{sc}(\lambda_0)}{e\phi^{inc}} \tag{18}$$

Similarly, we can define an internal quantum efficiency (IQE), which quantifies the ratio of the electron flux extracted from the TiO_2 film to the photon flux absorbed by the dye

$$\mathrm{IQE}(\lambda_0) = \frac{j_{sc}(\lambda_0)}{e\phi^{inc} f_{abs}(\lambda_0)} = \frac{\mathrm{EQE}(\lambda_0)}{f_{abs}(\lambda_0)} \tag{19}$$

where f_{abs} is the fraction of light absorbed by the dye in the film at wavelength λ_0 (eq 5).

The function $\mathrm{EQE}(\lambda)$ will depend on the direction of illumination, i.e., illumination from the TiO_2 substrate electrode (SE) side or from the electrolyte electrode (EE) side. However, the ratio of the EQE with SE and EE illumination is independent of η_{inj} and only depends on L and the excited dye state generation functions $G_{SE}^{dye,\delta}$ and $G_{EE}^{dye,\delta}$ for SE and EE illumination (see Supporting Information). From the optical model, we find accurate and validated values for $G_{SE}^{dye,\delta}$ and $G_{EE}^{dye,\delta}$. L could thus be extracted from experimental $\mathrm{EQE_{SE}}/\mathrm{EQE_{EE}}$ ratios using a single-parameter fit.[10,11,23] In this work, however, L is obtained from the current density ratios measured at different simulated solar spectral irradiance intensities. We favor this approach, since an irradiance with a white bias light, commonly used in the determination of EQEs, and the ensuing observed dependence of the quantum efficiency on this bias light intensity, are not modeled in the present work.

The parameters of the electrical model are L, η_{inj}, τ, N_c, and the difference $E_c - E_{F0}$ between the conduction band edge and the Fermi level in the dark. The only relevant parameters in the expressions for j_{sc} and $\mathrm{EQE}(\lambda)$ are η_{inj} and L. In our model j_{sc} and $\mathrm{EQE}(\lambda)$ do not depend on N_c, τ, and $E_c - E_{F0}$ (see Supporting Information). In this study, we will thus extract η_{inj} and L by comparing the simulations for j_{sc} to experimental data.

EXPERIMENTAL SECTION

Device Preparation. Complete test devices (Figure 1) were fabricated following standard procedures.[26] The FTO-coated top glass electrode (Nippon Sheet Glass, 10 Ω/□), was first immersed in an aqueous $TiCl_4$ solution to produce a thin TiO_2 charge blocking layer. An ~8 μm thick mesoporous layer of 20 nm sized TiO_2 particles was then screen-printed on the treated FTO electrode. The cell geometry was 0.4 × 0.4 cm^2 for test devices and 2 × 2 cm^2 for optical characterization. The TiO_2 film was sensitized with the ruthenium-based dye Z907[12] or C101[4] by overnight immersion in a 0.3 mM solution in a mixture of acetonitrile and *tert*-butanol (volume ratio 1:1). Chenodeoxycholic acid (0.03 mM) was added as coadsorbant to the C101 dye solution.[4] The cell was sealed with a thermally platinized FTO counter electrode (Pilkington, TEC 15, 15 Ω/□) using a 25 μm thick polymer spacer (Surlyn, DuPont). The void was then filled with an iodide/triiodide based electrolyte through a hole in the back electrode. The electrolyte consisted of 1.0 M 1,3-dimethylimidazolium iodide, 0.10 M guanidinium thiocyanate, 0.03 M iodine, and 0.5 M *tert*-butylpyridine in a mixture of acetonitrile and valeronitrile (volume ratio 85:15). In some cases, 0.05 M LiI was added to the electrolyte.

Optical Characterization of Layers. The thickness of the glass substrates (layers **1** and **6**) was measured with a digital micrometer. To determine the complex refractive index of the glass substrates ($\tilde{n}_1 = n_1 + ik_1$ and $\tilde{n}_6 = n_6 + ik_6$), the FTO films were removed with hydrochloric acid and zinc powder. The complex refractive indices were then extracted by fitting the Fresnel equations to measured transmittance and reflectance spectra (see Supporting Information). Transmittance and reflectance spectra were measured with a spectrophotometer (Varian Cary 5) equipped with an integrating sphere.

The thickness of the FTO films (layers **2** and **5**) was estimated from cross-sectional scanning electron micrographs. The real part of the refractive index of the top FTO layer **2** (n_2) was determined using a spectroscopic ellipsometer (SOPRA GES5E). Beforehand, the strongly textured surface of the FTO was polished using chemical mechanical planarization to minimize depolarization of the incident light beam.[27] n_2 was extracted by fitting the ellipsometric data to a Cauchy model, yielding values in good agreement with reported data.[27] Extraction of k_2 requires an accurate fitting model taking into account high-energy photon band gap absorption and low-energy photon absorption by free charge carriers. Our models were not accurate enough to extract reasonable values for k_2. Instead, k_2 was obtained by fitting measured transmittance and reflectance spectra using the optical model and the extracted n_2. For the bottom FTO film (layer **5**), the refractive index was set to $n_5 = n_2$, and k_5 was determined with the same method as k_2. The thin layer of platinum particles on the bottom electrode is virtually transparent, and its optical effect was thus neglected in this study.

The layer **3**, consisting of the dye-sensitized mesoporous anatase TiO_2 and the electrolyte permeating the pores, was treated as a Bruggeman effective medium[21] (see Optical Model). The TiO_2 film thickness was measured with a Alpha-Step 500 profilometer (KLA-Tencor), and its porosity was measured with a surface area analyzer (Micromeritics ASAP 2000) using the BET method (P = 0.68). For the bulk electrolyte medium **3a**, n_{3a} was taken from literature values for acetonitrile,[28] and k_{3a} was derived from

absorbance measurements of triiodide in acetonitrile, which is the only absorbing species in the electrolyte. For the fictitious TiO_2/dye medium **3b**, n_{3b} was taken from literature values for anatase.[29] The effective imaginary index k_3 was obtained from a four-flux model analysis[22] on transmittance and reflectance spectra of a simplified stack, where the two FTO electrodes (**1**/**2** and **5**/**6**) were replaced by soda-lime microscope glasses (Menzel Gläser).

The complex index of refraction of the electrolyte layer **4** was set to $\tilde{n}_4 = \tilde{n}_{3a}$.

Photovoltaic Characterization. The external quantum efficiency of test devices was measured using light from a 300 W xenon lamp (ILC Technology) focused through a Gemini-180 double monochromator. The photon flux of monochromatic light incident on the devices was measured using a calibrated silicon photodiode (independent calibrations performed at Frauenhofer ISE, Freiburg, Germany, and NREL, Golden, CO, USA) with a spectral response modified with a filter (KG5 Schott) to approximately match the absorption profile of the dyes. The monochromatic beam was chopped (4 Hz), and the modulated photocurrent was measured with a lock-in amplifier (SR 830, Stanford Research Systems). Additional white bias light from light emitting diodes with an intensity of about 10 mW cm^{-2} (10% sun) was provided during the measurement to generate a constant photocurrent in the cell.

The current−voltage curve of devices was measured by illuminating with light from a 450 W xenon lamp (LOT Oriel) matched to AM 1.5G sunlight irradiation with filters in the range of 350−750 nm (Schott K113 Tempax Sunlight Filter, Präzisions Glas & Optik GmbH, Germany). The beam intensity was calibrated with a silicon photodiode. The current and voltage were measured and controlled with a Keithley 2400 source meter. The incident light intensity was varied with wavelength-neutral wire mesh attenuators. The diffusion length L was obtained from single-parameter fits to the current density ratios measured at different simulated solar spectral irradiance intensities. The injection efficiency η_{inj} was then obtained from the known L and a single-parameter fit to the current density at different irradiance intensities.

All measurements were performed with a metal mask with an aperture area of 0.25 cm^2, which was slightly larger than the TiO_2 film area of 0.16 cm^2, to optimally capture the direct and diffuse incident light and to minimize measurement artifacts.[30]

RESULTS AND DISCUSSION

Optical Constants of Individual Layers. The extracted complex refractive indices of the six layers used as input for the optical model are shown in Figure 3.

The glass substrates (layers **1** and **6**) clearly have a higher refractive index than typical soda-lime microscope glass (n_M). This will increase the reflection losses at the first air/glass interface. Also, the extinction coefficient is quite high in the infrared region. For layer **6**, k_6 is about six times larger than in soda lime glass (k_M).

The complex refractive indices of the FTO films (layers **2** and **5**) are in good agreement with previously published data.[27] Though k_2 is about half as large as k_5, the absorption of the two films is in the same range, since layer **2** is about twice as thick as layer **5**.

The refractive index n_3 of the mesoporous medium TiO_2/dye/electrolyte (layer **3**) lies between the refractive index of anatase (~3.1 at 400 nm)[28] and acetonitrile (n_4), reflecting the volume ratios of the porous TiO_2 and the pore-filling electrolyte.

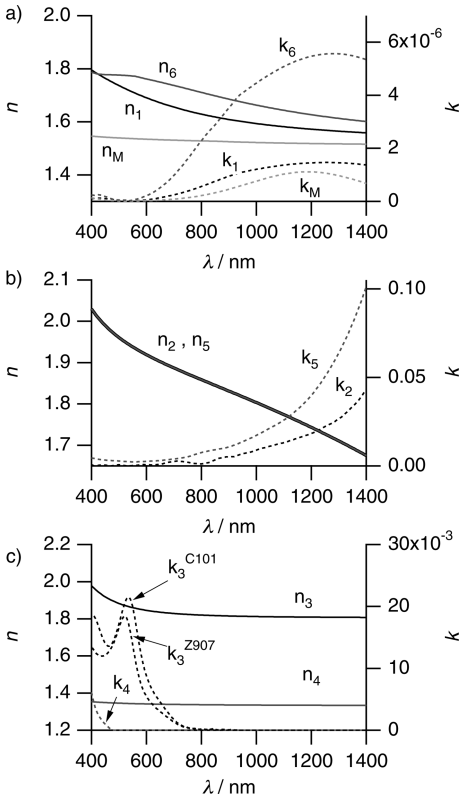

Figure 3. Extracted complex refractive indices of the layers **1**−**6** of a complete dye-sensitized solar cell used as input for the optical model. (a) Values for the glass substrates (**1** and **6**) and the reference soda-lime microscope glass (n_M, k_M) were obtained from fits of the Fresnel equations to measured transmittance and reflectance spectra. (b) The n of the FTO films (**2** and **5**) were derived from spectroscopic ellipsometry, and k from fits to transmittance and reflectance spectra with the determined n fixed. (c) The TiO_2/dye/electrolyte layer **3** was described with a Bruggemann effective medium approximation. k_3^{Z907} and k_3^{C101} were derived from a four-flux model analysis ($k_3^{Z907} = 1.84 \times 10^{-2}$ at 521 nm, $k_3^{C101} = 2.15 \times 10^{-2}$ at 534 nm). For the electrolyte layer **4**, the refractive index of acetonitrile and the extinction coefficient of triiodide were used.

The imaginary parts of the refractive index of layer **3**, k_3^{Z907} and k_3^{C101}, include the absorption of the dye (Z907 or C101) and triiodide in the pores (see Supporting Information for values of the absorption coefficients of the dye only). The magnitude and maxima agree well with reported values.[4] We note, that k_3^{Z907} and k_3^{C101} were extracted from a complete system (TiO_2/dye/solvent). Spectral shifts due to deprotonation of the dye after adsorption on the TiO_2 surface and due to polarization effects by the surrounding solvent are thus implicitly accounted for. The absorption in the electrolyte (k_4) is only due to triiodide. We confirmed with absorbance measurements that the other species in the electrolyte do not absorb in the range of interest.

The calculated reflectance (R) and transmittance (T) spectra of individual layers using the complex refractive indices of Figure 3 are compared to measured spectra in air in the Supporting Information. The agreement is excellent for the glass substrates. The surface of the top FTO (layer **2**) is strongly textured, causing substantial diffuse transmittance and reflectance of the top electrode (layers **1**/**2**) below 800 nm. In complete devices, however, the diffused light is absorbed by the dye, and only negligible diffusive components are visible in

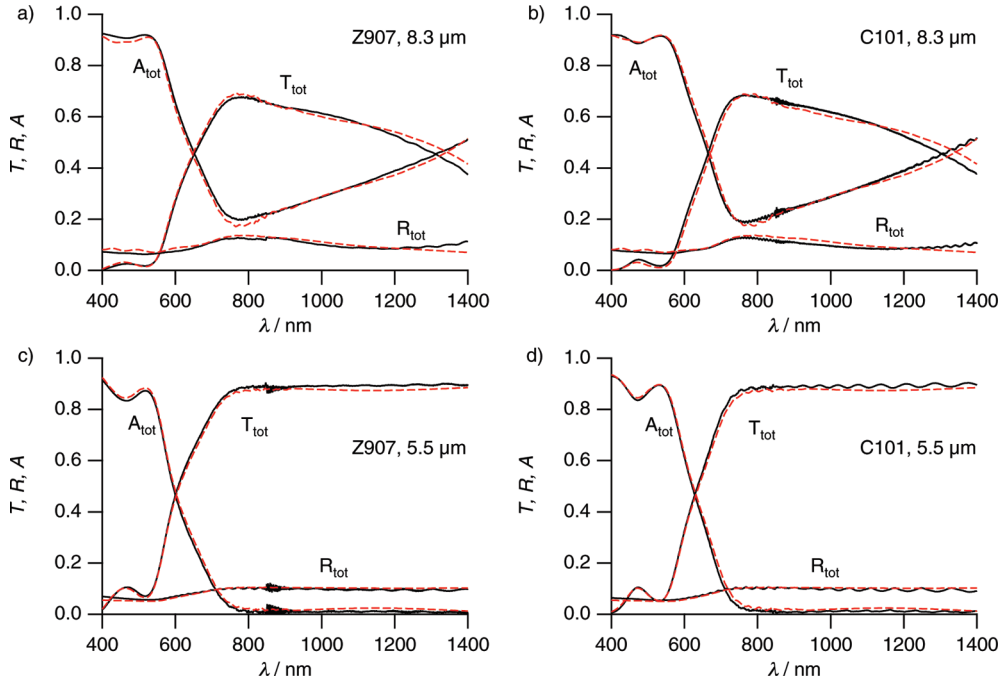

Figure 4. Measured and simulated total transmittance (T_{tot}), reflectance (R_{tot}), and absorption ($A_{tot} = 1 - T_{tot} - R_{tot}$) spectra of different stacks. Measurements are represented by bold dark lines and simulations by red dashed lines. (a, b) Complete device as shown in Figure 1 with Z907 dye (a) or C101 dye (b) (3.88 mm glass, 697 nm FTO, 8.3 μm TiO_2 with porosity $P = 0.68$, 16.7 μm bulk electrolyte, 360 nm FTO, 2.22 mm glass). (c, d) Simplified stack using microscope glass slides instead of FTO electrodes and Z907 dye (c) or C101 dye (d) (1.00 mm glass, 5.5 μm TiO_2 with porosity $P = 0.68$, 19.5 μm bulk electrolyte, 1.00 mm glass). The measured weak interference pattern above 800 nm in panels c and d is due to a small fraction of coherent light propagating in the TiO_2 film.

their measured T and R spectra. The spectra of the FTO electrode **1**/**2** cannot be well reproduced with a two-layer stack, since the optical model does not account for surface scattering. With the addition of a fictitious third Bruggemann effective mixed medium layer FTO/air of 55 nm ($P = 0.5$) the spectrum can be well simulated. The polished sample shows no more scattering but clear interference fringes instead, and the spectra can be well simulated with a two-layer model. The surface of the bottom electrode (layers **5**/**6**) is smooth (negligible diffuse components), but interference fringes are not well pronounced. In this case the simulation is less accurate.

Optical Simulation of Complete Devices. The optics of the complete device, as depicted in Figure 1, can be simulated once the thickness and the complex refractive index of each layer are known. The optical model calculates the total reflectance and transmittance, the absorptance in each layer, and the dye absorption rate in the film as a function of film thickness ($G^{dye}(x)$).

We first validate the optical model by comparing calculated and measured total transmittance (T_{tot}) and reflectance (R_{tot}) spectra of different devices. In Figure 4a and Figure 4b we compare the spectra of a complete device with an 8.3 μm thick TiO_2 film sensitized with Z907 and C101 dye, respectively. The illumination is incident from the TiO_2 substrate electrode (SE) side. The measured and simulated spectra are in good agreement. We attribute the small differences mainly to the slightly inaccurate optical constants of the FTO electrodes (see Supporting Information). Figure 4c and Figure 4d show the measured and simulated T_{tot} and R_{tot} spectra of a simplified stack with a 5.5 μm thick TiO_2 film sensitized with Z907 and C101 dye, respectively, sandwiched between two 1 mm thick soda-lime glass microscope slides. In this case, the agreement between the measurement and the simulation is excellent. The optics in the mixed mesoporous medium can thus be well described by a Bruggemann effective medium approach.

For illumination of a complete device from the electrolyte electrode side (EE), which is shown in the Supporting Information, the model slightly overestimates the total reflectance of the complete device and underestimates the total absorptance for $\lambda <$ 700 nm (e.g., at $\lambda = 520$ nm: $R_{meas} = 0.096$, $R_{sim} = 0.128$, $A_{meas} = 0.857$, and $A_{sim} = 0.887$, i.e., a misestimation of about 3%). This is clearly due to the inaccurate refractive indices of the back electrode (layers **5** and **6**), as the simulation of a device with microsocpe glass slides instead of FTO electrodes shows excellent agreement with the measurements.

Optical Loss Analysis. The optical model is very helpful to quantify the different optical loss channels. This is exemplified for a device with an 8.3 μm TiO_2 film and Z907 dye in Figure 5. The calculated R_{tot}, the absorptance in each layer (A_i, where $1 \leq i \leq 6$), and T_{tot} are shown in a stack diagram for illumination incident from the substrate electrode (SE, Figure 5a) or the electrolyte electrode (EE, Figure 5b) side.

We find $R_{tot} + \Sigma A_i + T_{tot} = 1$ in accordance with energy conservation. T_{tot} is independent of illumination direction. R_{tot} and A_i, however, strongly depend on the illumination direction. We see for instance, that the reflection loss for EE illumination is larger than that for SE illumination since the optical contrast is higher at the air/**6** interface ($n_6 > n_1$). The absorptance losses in the glass substrates and in the FTO films in the visible region are uncritical for SE illumination but are not negligible for EE illumination, which is mainly due to the high values of k_5 and k_6. In the infrared region the absorptance losses are substantial. The accurate, layer-resolved quantification of these losses could become useful for the optimization of tandem solar cells, where a

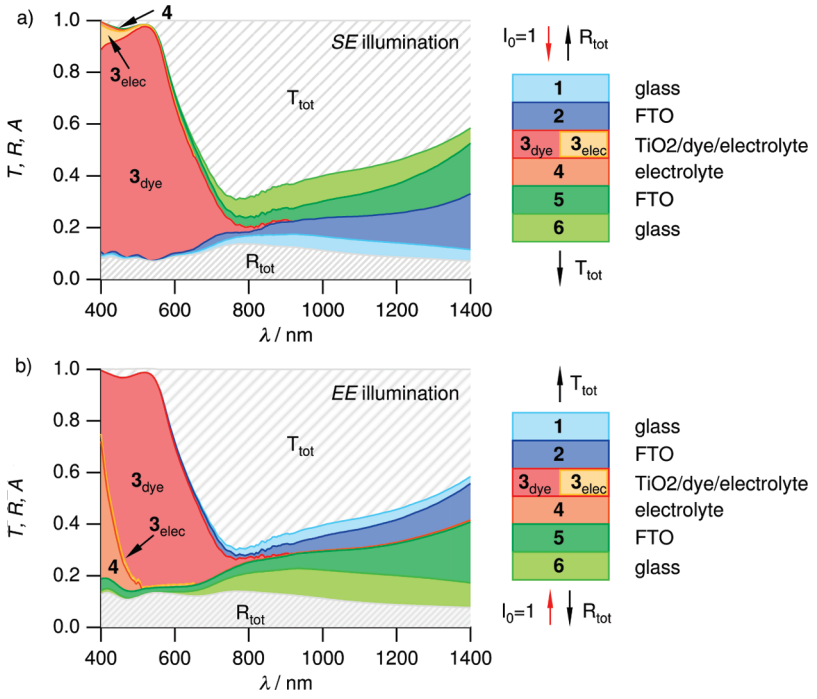

Figure 5. Detailed optical loss analysis of a DSC stack as in Figure 1 (8.3 μm of TiO_2, Z907 dye). The calculated total reflectance R_{tot}, the absorptance in each layer A_i ($1 \le i \le 6$, labeled with bold numbers in the graphs), and the total transmittance (T_{tot}) are stacked in the graphs and add up to 1. Simulated for substrate electrode (SE, a) or electrolyte electrode (EE, b) side illumination. The absorptance of the dye and the electrolyte in the mesoporous layer **3** is separated in the graphs (labeled **3** dye and **3** elec, respectively).

DSC is used as top cell, and the transmitted near-infrared light is absorbed by a bottom cell.[31]

The absorptance in the photoactive layer **3** is separated into the absorptance by the dye, $A_{dye}(\lambda) = f_{abs}(\lambda)$, and the absorptance by the remaining components, A'_3 (mostly triiodide in the pores, but also some impurities in the TiO_2, see Supporting Information. A_{dye} and A'_3 are labeled as $\mathbf{3}_{dye}$ and $\mathbf{3}_{elec}$ in the figures, respectively. As can be seen in Figure 5a, light absorption by triiodide in the pores ($\mathbf{3}_{elec}$) is not negligible for SE illumination. Only very little light is absorbed in the subsequent bulk electrolyte layer (**4**). For EE side illumination Figure (5b), absorption by the bulk electrolyte layer is substantial and considerably attenuates the amount of light, which can be absorbed by the dye molecules. Absorption by triiodide in the pores is marginal. Bulk electrolyte absorption is a real concern for DSCs that require EE side illumination, for instance if a metal foil substrate electrode is used. This loss can only be reduced by decreasing the effective volume of the electrolyte, for instance by replacing the bulk layer with a mesoporous SiO_2 layer infiltrated with the redox mediator.[32]

Dye Absorption rate $G^{dye}(x)$. With the optical model we can find accurate values for the rate of absorption of photons by the dye per volume element as a function of TiO_2 film thickness ($G^{dye}(x)$). In Figure 6, $G^{dye}(x)$ is plotted for a device with Z907 or C101 dye (11.2 μm TiO_2) for AM 1.5G illumination (1000 W m^{-2}) from the SE or EE side. For comparison, we show an exponential Lambert–Beer type absorption, as frequently used in other DSC models.[10,11,15] For SE and EE illumination, the generation rate for excited dye states is approximated by

$$G_{SE} = (1 - R_{NSG})\alpha_{dye}\phi_{inc}e^{-(\alpha_{dye} + \alpha_{redox})x} \quad (20)$$

and

$$G_{EE} = (1 - R_{TEC})T_{Pt}T_{redox}\alpha_{dye}\phi_{inc}e^{-(\alpha_{dye} + \alpha_{redox})(d - x)} \quad (21)$$

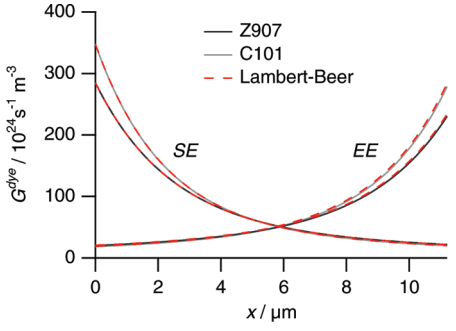

Figure 6. Comparison of the dye absorption rate $G^{dye}(x)$ for dyes Z907 and C101 for SE and EE illumination calculated with the optical model. The incident photon flux is AM 1.5G irradiance (100 mW cm^{-2}).

where R_{NSG} and R_{TEC} are the total reflectance of the front and back electrode measured in air (see Supporting Information), α_{dye} and α_{redox} are the absorption coefficients of the dye and the triiodide in the pores, respectively, T_{Pt} is the transmittance of the Pt layer on the counterelectrode (for our thermal Pt depositions $T_{Pt} \sim 1$), and T_{redox} is the transmittance of the electrolyte bulk layer **4**.

We find that G^{dye} is quite similar for both calculation methods. For Z907, the maximum short-circuit current obtained with the ray tracer is 14.72 mA cm^{-2} for SE illumination and 12.53 mA cm^{-2} for EE illumination. With the Lambert–Beer calculation one finds 14.46 mA cm^{-2} for SE illumination and 12.89 mA cm^{-2} for EE illumination. These differences are within experimental error.

We can thus conclude that the Lambert–Beer type generation function used by others[10,11,15] is approximately valid. However,

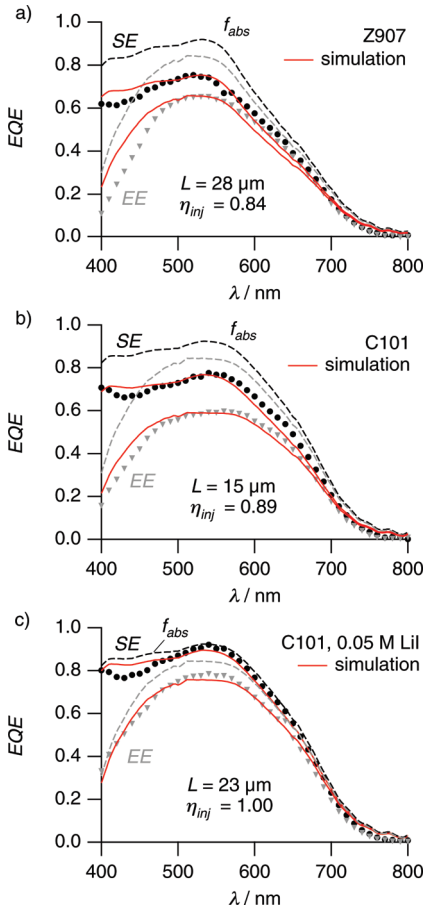

Figure 7. Measured EQE of different cells for illumination from the SE side (dark circles) or the EE side (gray triangles). TiO_2 film thickness d = 11.2 μm. (a) Z907 dye, (b) C101 dye, (c) C101 dye with 0.05 M Li in the electrolyte. Cells were measured with white bias light with an intensity of about 10 mW cm^2. The calculated fraction of absorbed light f_{abs} (dashed lines) is shown for both illumination cases. Red bold lines are best fits to experimental data.

the optical model based on the ray-tracing algorithm provides a valuable tool for the detailed analysis of optical losses caused by each layer of the cell, as has been demonstrated in the previous paragraph.

Extracting L and η_{inj} with the Coupled Optical and Electrical Model. The dye absorption rate $G^{dye}(x)$, which is accurately calculated for SE and EE illumination with the optical model, is now inserted as a source term into the continuity equation for free electrons to calculate the steady-state behavior of the device at short-circuit, i.e., the external quantum efficiency (EQE) and the short-circuit current density (j_{sc}). The free fitting parameters are the diffusion length L and the injection efficiency η_{inj}.

We analyzed three different cell systems with a TiO_2 film thickness of d = 11.2 μm: (1) Z907 dye, (2) C101 dye, and (3) C101 dye, and 0.05 M Li in the electrolyte. L was determined with a single-parameter fit from the ratio of the measured short-circuit current densities for SE and EE illumination using a simulated solar spectrum irradiance (AM1.5G). η_{inj} was subsequently determined with the fixed L by a single-parameter fit to the short-circuit current for SE illumination vs incident illumination intensity.

In Figure 7, the measured and calculated EQEs of these cell systems is plotted for illumination from the SE or EE side. The fraction of absorbed light by the dye, f_{abs} = EQE_{max} is also shown. The extracted parameters L and η_{inj} for each system are given in Table 1. The maximum obtainable photocurrent for AM 1.5G irradiance ($j_{max}^{AM1.5G}$) calculated with the optical model, the measured current under Xe lamp illumination (j_{meas}^{Xe}), and the calculated current for AM 1.5G ($j_{calc}^{AM1.5G}$), from the electrical model and the respective L and η_{inj}, are also tabulated.

For the systems Z907 and C101 without Li ions in the electrolyte, there is a large difference between the maximum obtainable and the measured current densities. For the device with Z907, under SE side illumination, 91% of the incident photons are absorbed by the dye at 520 nm, but only 75% of the photons are extracted as electrons in a real device. This corresponds to an *absorbed photon-to-current conversion efficiency* or *internal quantum efficiency* (IQE) of 82%. In contrast, the device with the high absorptivity C101 dye and additional lithium in the electrolyte has an IQE of 97% at 520 nm under SE side illumination (see Table 1).

Absorbed light to current conversion losses may be due to the following mechanisms:

1. Dye aggregates are present that absorb light but do not inject into the TiO_2.
2. Excited dyes relax back to their ground state and do not inject ($\eta_{inj} < 1$).
3. Injected electrons in the TiO_2 conduction band recombine with oxidized dye species.
4. Injected electrons recombine with triiodide at the TiO_2/electrolyte interface.

Dye aggregates are improbable since desorption studies suggest a TiO_2 surface coverage of ≈100%.

The photoinduced injection of electrons from the excited dye into the TiO_2 conduction band seems to be restricted for both dye systems. A low injection yield for Z907 ($\eta_{inj} \approx 0.9$) has also been observed with laser transient absorbance measurements in ionic liquid. However η_{inj} approached unity if Li ions were added to the electrolyte.[33] This "Li-effect" was also observed with other ruthenium bipyridine complexes[34] and with time-resolved single photon counting[35] and other EQE ratio studies.[11] In another study,[36] the increase in injection efficiency was observed to come along with a red shift in the IPCE spectrum, indicating a wavelength-dependent η_{inj}. The improved injection yield is attributed to a lowering of the TiO_2 conduction band subsequent to surface adsorption of Li^+ ions, which enhances the driving force for injection. In accordance, we observe that η_{inj} approaches unity when LiI is added to the C101 system.

Following injection, electrons may recombine with the dye cation. This recombination mechanism is currently not implemented in the model. Nanosecond transient absorption studies on the Z907 system indicate that a significant fraction of electrons (10−15%) is recaptured by the dye cations.[12] However, this recombination pathway does not influence the calculated IQE. To date, there exist no dye recombination studies for C101, but a regeneration yield of 99% (i.e., 1% of the injected electrons recombine with the cation) has been reported for a similar system with extended conjugation in the hydrophobic system.[37,38]

The recombination of electrons in the TiO_2 with I_3^- is related to the magnitude of the diffusion length L. We found lower values for L in the C101 system than in the Z907 system. The values for L in C101 devices are in relatively good agreement with those found in another study.[39] Provided that the free electron diffusion coefficient D is independent of dye type and electrolyte composition, the lower values for L indicate that recombination

Table 1. Comparison of Maximum ($j_{max}^{AM1.5G}$), Measured (j_{meas}^{Xe}), and Calculated ($j_{calc}^{AM1.5G}$) Short-Circuit Photocurrent Densities for Different Cell Systems under Front (SE) or Back (EE) Side Illumination[a]

dye	irrad.	Li (M)	$j_{max}^{AM1.5G}$ (mA cm^{-2})	j_{meas}^{Xe} (mA cm^{-2})	$j_{calc}^{AM1.5G}$ (mA cm^{-2})	L (μm)	η_{inj}	IQE @520 nm
Z907	SE		14.7	11.9	11.9	28	0.84	0.82
	EE		12.5	10.0	9.9	28	0.84	0.78
C101	SE		15.9	12.6	12.8	15	0.89	0.83
	EE		13.6	10.1	9.8	15	0.89	0.70
C101	SE	0.05	15.9	15.1	15.1	23	1.00	0.97
	EE	0.05	13.6	12.1	12.3	23	1.00	0.90

[a] TiO_2 film thickness d = 11.2 μm. L and $\mathbf{h}_{inj}$ are best fits to experimental j_{sc} data. The internal quantum efficiency is defined as IQE = EQE/f_{abs}.

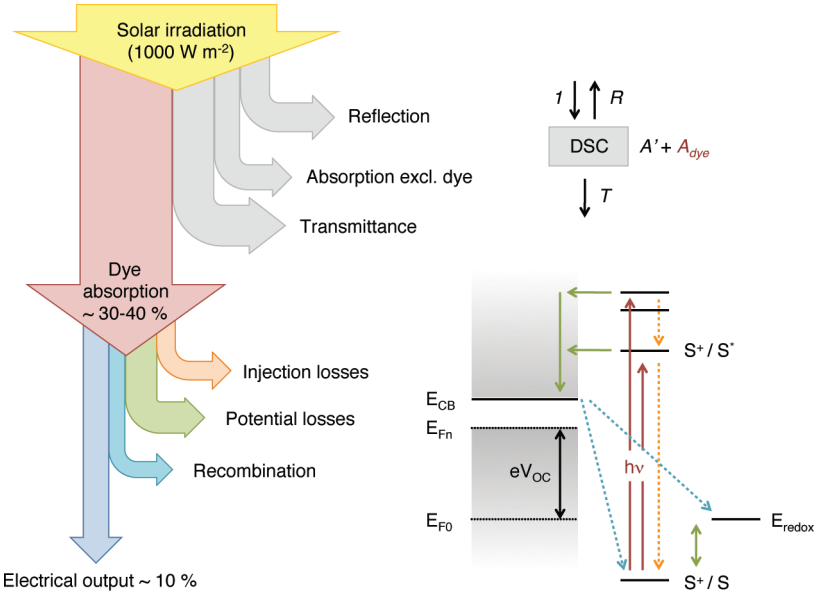

Figure 8. Schematic of the various optical and electrical losses in a DSC. A large fraction of the incident irradiation is lost due to reflection, absorption by materials other than the dye, and transmittance. Excited dye states either relax back to the ground state (injection loss) or inject an electron into the TiO_2 conduction band. The final potential difference at the electrodes is given by the difference between the quasi-Fermi level E_{Fn} and the redox energy level in the electrolyte. At the maximum operating point, a good DSC finally converts about 10% of the incident irradiation into electrical power.

with I_3^- is faster in the C101 system than in the Z907 system. Recombination might be enhanced by the formation of an iodine/dye complex at the thiophene units of the C101 ligands, which would increase the concentration of electrolyte species close to the TiO_2 surface.[40,41] We also observed that L increases in the C101 system upon addition of Li ions. This is likely due to improved charge transport in the film because of electrostatic shielding by the positively charged Li ions.

Comprehensive Power Loss Analysis. A particularly instructive feature of the coupled optical and electrical DSC model is the quantification of optical and electric losses.

As illustrated in Figure 8, only a small fraction of the total incident solar spectrum is converted into electric power (~10−11% in high-efficiency DSCs). A large part of the solar flux is lost due to reflection, absorption in materials other than the dye, and transmittance through the cell. Excited dye states may relax back to the ground state (injection loss). After injection, at least half of the photon energy is lost due to thermalization of the injected electron to the TiO_2 conduction band level and due to the offset between the dye ground state and the redox energy level. Also the electron may recombine with I_3^- in the electrolyte or with dye cations. This back reaction limits the electron concentration in the film at open circuit and determines the position of the quasi-Fermi level and the magnitude of the photovoltage.

In the model, losses are quantified in terms of power per unit area. Optical losses are calculated by integrating the product of total reflectance (R_{tot}), transmittance (T_{tot}), and absorptance in materials other than the dye ($A' = 1 - R_{tot} - T_{tot} - f_{abs}$), respectively, with the incident spectral irradiance.

The total integrated external reflection losses are

$$P_R = \int_{\lambda_{min}}^{\lambda_{max}} R_{tot}(\lambda) I_0(\lambda)\, d\lambda \qquad (22)$$

the total integrated transmission losses are

$$P_T = \int_{\lambda_{min}}^{\lambda_{max}} T_{tot}(\lambda) I_0(\lambda)\, d\lambda \qquad (23)$$

and the integrated losses due to absorption in materials other than dye are

$$P_A = \int_{\lambda_{min}}^{\lambda_{max}} A'(\lambda) I_0(\lambda)\, d\lambda \qquad (24)$$

Injection losses are quantified using

$$P_{\mathrm{inj}} = \int_{\lambda_{\min}}^{\lambda_{\max}} (1 - \eta_{\mathrm{inj}}) f_{\mathrm{abs}}(\lambda) I_0(\lambda)\, \mathrm{d}\lambda \quad (25)$$

Recombination and potential losses are evaluated at the maximum power point (MPP)

$$P_{\mathrm{rec}} = \int_0^d U(x)(E_{Fn}^{\mathrm{mpp}}(x = 0) - E_{\mathrm{F0}})\, \mathrm{d}x \quad (26)$$

$$P_{\mathrm{pot}} = \int_{\lambda_{\min}}^{\lambda_{\max}} \eta_{\mathrm{inj}} f_{\mathrm{abs}}(\lambda) I_0(\lambda) \left[1 - \frac{\lambda}{hc}(E_{Fn}^{\mathrm{mpp}}(x = 0) - E_{\mathrm{F0}})\right] \mathrm{d}\lambda \quad (27)$$

Here, $U(x)$ is the recombination rate given by

$$U(x) = \frac{n(x) - \overline{n}}{\tau} \quad (28)$$

and $E_{Fn}^{\mathrm{mpp}}(x = 0)$ is the calculated quasi-Fermi level at the anode under MPP conditions. The potential losses P_{pot} are calculated from the energy difference between the harvested photons and the electrons extracted at the anode. We took also into account the series resistance loss

$$P_{R_s} = R_s j_{\mathrm{mpp}}^2 \quad (29)$$

where R_s is the series resistance in units of Ωm^2. R_s is found from a fit of the simulated total power output to the measured one. The power output is given by

$$P_{\mathrm{out}} = j_{\mathrm{mpp}} V_{\mathrm{mpp}} \quad (30)$$

Instead of quantifying the losses in units of power P, they can alternatively be given in terms of current density J (in units of mA cm^{-2}). This is obtained from integration over the incident photon flux, instead of the irradiance, and multiplication by the elementary charge.

We give a sample calculation for the two devices treated previously (TiO_2 film thickness d = 11.2 μm): Z907 with L = 28 μm and η_{inj} = 0.84 and C101 with Li in the electrolyte, L = 23 μm, and η_{inj} = 1.00. The electron lifetime for electrons in the TiO_2 conduction band is set to τ = 2.4 ms for the Z907 device and τ = 0.4 ms for the C101 device . In this way, we obtain calculated open circuit voltages in agreement with the measurements ($V_{\mathrm{oc}}^{\mathrm{calc}}$ = 829.7 mV for Z907 and $V_{\mathrm{oc}}^{\mathrm{calc}}$ = 724.6 mV for C101). We note that trap distribution parameters must not be known for steady-state calculations. The incident irradiance is AM 1.5G from the TiO_2 side. The losses are quantified in Table 2.

The losses are integrated from $\lambda_{\min}$ = 400 nm (in order to avoid band gap excitation of the semiconductor) to $\lambda_{\max}$ = 1400 nm (since the materials are not characterized beyond this wavelength). The AM 1.5G incident irradiance in this range is 872 W m^{-2}, the remaining 128 W m^{-2} are not assigned to any specific loss channel. A large fraction of the incident flux is lost due to reflection, transmittance, absorptance by materials, and insufficient injection. These flux losses amount to 58% for the Z907 system and 50% for the C101 system. For these particular systems, losses could be reduced with antireflecting layers and back reflectors (e.g., a layer of large scattering TiO_2 particles behind the "transparent" mesoporous layer, as used in high efficiency cells). Injection losses can constitute a significant loss channel (5.5% with Z907). After injection, a major fraction of the photon energy is lost due to potential losses (about 20−30%). Surprisingly, only a negligible fraction of energy is lost due to charge recombination with I_3^- in the electrolyte (≈1%). However, the position of the quasi-Fermi level at the MPP, used for the calculation of losses in eq 26 and eq 27, also depends on the recombination rate, and it is somewhat difficult to unambiguously differentiate between recombination and potential losses. Nevertheless, these losses must be addressed with the investigation of new redox mediators (with a redox energy level closer to the dye ground state level), the development of tandem systems to reduce thermalization losses, and strategies to reducing recombination (e.g., coadsorbants and core−shell structures). Finally, we find a power output of about 75.9 W m^{-2} for the Z907 system and 78.3 W m^{-2} for the C101 system, which corresponds to a photovoltaic power conversion efficiency of 7.59% (FF = 0.766) and 7.83% (FF = 0.711), respectively. The measured photovoltaic parameters were η = 7.6% for the Z907 system (V_{oc} = 830 mV, J_{sc} = −11.9 mA cm^{-2}, FF = 0.77) and η = 7.8% for the C101 system (V_{oc} = 724 mV, J_{sc} = −15.1 mA cm^{-2}, FF = 0.71). The good agreement between the measured and simulated fill factors was achieved for a series resistance of R_s = 7.3 Ω cm^2 for both device types.

In our opinion, such a comprehensive loss analysis, which is now possible with the optoelectric DSC model, is an important tool to assess the potential for optimization of the DSC and to identify the most promising optimization strategies.

Table 2. Quantification of Different Loss Channels with the Optoelectric DSC Simulator[a]

loss channel	dye	P/W m^{-2}	J/mA cm^{-2}	percent
incident spectrum		872.0	51.5	87.2
reflection	Z907	85.2	5.2	8.52
	C101	83.7	5.1	8.37
transmittance	Z907	317.3	22.4	31.73
	C101	298.5	21.4	29.85
absorptance	Z907	126.7	9.3	12.67
	C101	122.4	9.1	12.24
injection	Z907	54.9	2.3	5.49
	C101	0.0	0.0	0.0
recombination	Z907	6.8	0.9	0.68
	C101	10.0	1.5	1.0
potential	Z907	196.0		19.6
	C101	264.3		26.43
series resistance	Z907	9.6		0.96
	C101	15.1		1.51
output	Z907	75.9	11.4	7.59
	C101	78.3	14.4	7.83

[a] Calculations are for devices with a TiO_2 film thickness d = 11.2 μm and dye Z907 (L = 28 μm, η_{inj} = 0.84) or C101 (L = 23 μm, η_{inj} = 1.00). The series resistance for both devices is $\mathbf{R}_s$ = 7.3 Ω cm^2. The incident irradiance is AM 1.5G from the TiO_2 side. Losses are integrated from λ = 400 to 1400 nm. Recombination and potential losses are evaluated at the maximum power point.

CONCLUSIONS

We have developed an experimentally validated and accurate optical model for dye-sensitized solar cells. This model allows us to correctly compute the dye absorption function for any incident

spectrum, illumination direction, or stack assembly (e.g., including antireflective coatings or back reflectors). Hence, the internal quantum efficiency of test devices—an important cell characteristic that was difficult to assess so far—can be accurately computed. By coupling the results of the optical model to an electrical model for charge generation, transport, and recombination, intrinsic parameters (such as the diffusion length and the injection efficiency) can be extracted from steady-state measurements. With the coupled model, the different optical and electric losses can be quantified. This comprehensive loss analysis paves the way for a systematic, model-assisted, optimization of dye-sensitized solar cells.

The presented model should be regarded as a basic framework for the accurate description of test devices. It can be extended to simulate time-dependent measurements, such as current or voltage transients and electrochemical impedance spectra. Also, the model can be further developed to account for scattering of light (to describe high-efficiency cells) and nonlinear charge recombination (to accurately describe nonlinear cells close to open-circuit condition). Nevertheless, the model as presented here is already a valuable tool for understanding the device optics and physics in greater depth, to identify dominant loss channels, and to optimize device parameters (e.g., optimal TiO_2 film thickness).

■ ASSOCIATED CONTENT

Supporting Information. Dependence of EQE ratio on bias light intensity, absorption coefficient of the mixed TiO_2/dye medium derived with a four-flux analysis, general solution of the linear continuity equation for conduction band electrons, and comparison of measured and simulated transmittance and reflectance spectra. This material is available free of charge via the Internet at http://pubs.acs.org.

■ AUTHOR INFORMATION

Corresponding Author

*E-mail: juergen.schumacher@zhaw.ch.

Present Addresses

¶ewz, Tramstrasse 35, CH-8050 Zurich, Switzerland.

■ ACKNOWLEDGMENT

We thank Pascal Comte for TiO_2 film preparation, Peng Wang for a C101 dye sample, Shaik M. Zakeeruddin for electrolyte and dye solution preparation, Frédéric Sauvage for taking the scanning electron micrographs, Didier Bouvet for mechanical polishing of the front FTO electrode, and Philippe Langlet for assistance with ellipsometry measurements (all EPFL). Financial support by the GERBERT RÜF STIFTUNG (project No. GRS-064/07) and the Swiss National Science Foundation (project No. NF 20020-125163/1) is gratefully acknowledged.

■ REFERENCES

(1) Grätzel, M. *Nature* **2001**, *414*, 338–344.
(2) Nazeeruddin, M. K.; De Angelis, F.; Fantacci, S.; Selloni, A.; Viscardi, G.; Liska, P.; Ito, S.; Takeru, B.; Grätzel, M. *J. Am. Chem. Soc.* **2005**, 16835–16847.
(3) Chiba, Y.; Islam, A.; Watanabe, Y.; Komiya, R.; Koide, N.; Han, L. *Jpn. J. Appl. Phys., Part 2* **2006**, *45*, L638–L640.
(4) Gao, F.; Wang, Y.; Shi, D.; Zhang, J.; Wang, M. K.; Jing, X. Y.; Humphry-Baker, R.; Wang, P.; Zakeeruddin, S. M.; Grätzel, M. *J. Am. Chem. Soc.* **2008**, *130*, 10720–10728.
(5) http://www.pv.unsw.edu.au/links/products/pc1d.asp.
(6) Burgelman, M.; Verschraegen, J.; Degrave, S.; Nollet, P. *Prog. Photovoltaics* **2004**, *12*, 143–153.
(7) Häusermann, R.; Knapp, E.; Moos, M.; Reinke, N. A.; Flatz, T.; Ruhstaller, B. *J. Appl. Phys.* **2009**, *106*, 104507–9.
(8) http://www.pecsim.ch.
(9) Peter, L. M. *J. Phys. Chem. C* **2007**, *111*, 6601–6612.
(10) Halme, J.; Boschloo, G.; Hagfeldt, A.; Lund, P. *J. Phys. Chem. C* **2008**, *112*, 5623–5637.
(11) Barnes, P. R. F.; Anderson, A. Y.; Koops, S. E.; Durrant, J. R.; O'Regan, B. C. *J. Phys. Chem. C* **2009**, *113*, 1126–1136.
(12) Wang, P.; Zakeeruddin, S. M.; Moser, J. E.; Nazeeruddin, M. K.; Sekiguchi, T.; Grätzel, M. *Nat. Mater.* **2003**, *2*, 402–407.
(13) Barnes, P. R. F.; O'Regan, B. C. *J. Phys. Chem. C* **2010**, *114*, 19134–19140.
(14) Bisquert, J.; Mora-Seró, I. *J. Phys. Chem. Lett.* **2010**, *1*, 450–456.
(15) Villanueva-Cab, J.; Wang, H.; Oskam, G.; Peter, L. M. *J. Phys. Chem. Lett.* **2010**, 748–751.
(16) Bisquert, J.; Fabregat-Santiago, F.; Mora-Seró, I.; Garcia-Belmonte, G.; Giménez, S. *J. Phys. Chem. C* **2009**, *113*, 17278–17290.
(17) Schumacher, J. O. *PhD thesis*, University of Konstanz, 2000.
(18) Donges, A. *Eur. J. Phys.* **1998**, *19*, 245–249.
(19) Born, M.; Wolf, E. *Principles of optics: electromagnetic theory of propagation, interference and diffraction of light*, 7th ed.; Cambridge University Press: Cambridge, U.K., 1999.
(20) Centurioni, E. *Appl. Opt.* **2005**, *44*, 7532–7539.
(21) Bruggeman, D. A. G. *Ann. Phys.* **1935**, *24*, 636–664.
(22) Rothenberger, G.; Comte, P.; Grätzel, M. *Sol. Energy Mater. Sol. Cells* **1999**, *58*, 321–336.
(23) Soedergren, S.; Hagfeldt, A.; Olsson, J.; Lindquist, S.-E. *The J. Phys. Chem.* **1994**, *98*, 5552–5556.
(24) Bisquert, J.; Vikhrenko, V. S. *J. Phys. Chem. B* **2004**, *108*, 2313–2322.
(25) Sze, S. M.; Ng, K. K. *Physics of Semiconductor Devices*, 3rd ed.; John Wiley & Sons, Inc.: 2006.
(26) Ito, S.; Murakami, T. N.; Comte, P.; Liska, P.; Grätzel, C.; Nazeeruddin, M. K.; Grätzel, M. *Thin Solid Films* **2008**, *516*, 4613–4619.
(27) Paulson, P. D.; Hegedus, S. S. *J. Appl. Phys.* **2004**, *96*, 5469–5477.
(28) Kozma, I. Z.; Krok, P.; Riedle, E. *J. Opt. Soc. Am. B* **2005**, *22*, 1479–1485.
(29) Tang, H.; Berger, H.; Schmid, P. E.; Lévy, F. *Solid State Commun.* **1994**, *92*, 267–271.
(30) Ito, S.; Nazeeruddin, M. K.; Liska, P.; Comte, P.; Charvet, R.; Péchy, P.; Jirousek, M.; Kay, A.; Zakeeruddin, S. M.; Gratzel, M. *Prog. Photovoltaics* **2006**, *14*, 589–601.
(31) Wenger, S.; Seyrling, S.; Tiwari, A. N.; Grätzel, M. *Appl. Phys. Lett.* **2009**, *94*, 173508.
(32) Ito, S.; Zakeeruddin, S. M.; Comte, P.; Liska, P.; Kuang, D.; Grätzel, M. *Nat. Photonics* **2008**, *2*, 693–698.
(33) Wang, P.; Zakeeruddin, S. M.; Moser, J.-E.; Grätzel, M. *J. Phys. Chem. B* **2003**, *107*, 13280–13285.
(34) Tachibana, Y.; Haque, S. A.; Mercer, I. P.; Moser, J. E.; Klug, D. R.; Durrant, J. R. *J. Phys. Chem. B* **2001**, *105*, 7424–7431.
(35) Koops, S. E.; O'Regan, B. C.; Barnes, P. R. F.; Durrant, J. R. *J. Am. Chem. Soc.* **2009**, *131*, 4808–4818.
(36) Jennings, J. R.; Wang, Q. *J. Phys. Chem. C* **2010**, *114*, 1715–1724.
(37) Wang, P.; Klein, C.; Humphry-Baker, R.; Zakeeruddin, S. M.; Grätzel, M. *J. Am. Chem. Soc.* **2004**, *127*, 808–809.
(38) Kuang, D. B.; Ito, S.; Wenger, B.; Klein, C.; Moser, J. E.; Humphry-Baker, R.; Zakeeruddin, S. M.; Grätzel, M. *J. Am. Chem. Soc.* **2006**, *128*, 4146–4154.
(39) Barnes, P. R. F.; Liu, L.; Li, X.; Anderson, A. Y.; Kisserwan, H.; Ghaddar, T. H.; Durrant, J. R.; O'Regan, B. C. *Nano Lett.* **2009**, *9*, 3532–3538PMID: 19645462.

(40) Marinado, T.; Nonomura, K.; Nissfolk, J.; Karlsson, M. K.; Hagberg, D. P.; Sun, L.; Mori, S.; Hagfeldt, A. *Langmuir* **2010**, *26*, 2592–2598.
(41) O'Regan, B. C.; López-Duarte, I.; Martnez-Daz, M. V.; Forneli, A.; Albero, J.; Morandeira, A.; Palomares, E.; Torres, T.; Durrant, J. R. *J. Am. Chem. Soc.* **2008**, *130*, 2906–2907.